DOI: 10.13009/EUCASS2023-330
Aerospace Europe Conference 2023 – 10TH EUCASS – 9TH CEAS

Aeroelastic Demonstrator and Methodology for Experimental Investigation of Propeller Aerodynamic Derivatives

Jiří Čečrdle[*†]
* *Czech Aerospace Research Centre (VZLU)*
Beranovych 130, Prague, 199 05, Czechia
cecrdle@vzlu.cz
[†] Corresponding Author

Abstract
Whirl flutter is a specific type of flutter instability, for which the experimental validation of analytical results is required. To determine propeller aerodynamic forces on a vibrating propeller, aerodynamic derivatives are used. Described demonstrator represents a sting-mounted nacelle with a motor and propeller. It includes engine pitch and yaw degrees-of-freedom. For the measurement, a single degree-of-freedom model is used and blocking of either pitch or yaw movement is provided. Pitching moment and vertical force due to the pitch angle and pitching moment and vertical force due to the yaw angle derivatives are investigated. Measured quantities include pitch and yaw angles and pivot moments.

1. Introduction

Whirl flutter is a specific type of aeroelastic flutter instability, which may appear on turboprop aircraft due to the effect of rotating parts, such as a propeller or a gas turbine engine rotor. Rotating mass generates additional forces and moments and increases the number of degrees-of-freedom. Rotating propellers also cause an aerodynamic interference effect between a nacelle and a wing. Whirl flutter instability is driven by motion-induced unsteady aerodynamic propeller forces and moments acting at the propeller plane. It may cause unstable vibration, which can lead to failure of an engine installation or an entire wing.
The propeller whirl flutter phenomenon was analytically discovered by Taylor and Browne in 1938 [1]. The next pioneering work was performed by Ribner, who set the basic formulae for the aerodynamic derivatives of propeller forces and moments due to the motion and velocities in pitch and yaw in 1945 [2, 3]. After the accidents of two Lockheed L-188 C Electra II airliners in 1959 and 1960 [4], the importance of the whirl flutter phenomenon on practical applications was recognized.
The complicated physical principle of whirl flutter requires experimental validation of the analytically results obtained, especially due to the unreliable analytical solution of the propeller aerodynamic forces. Further, structural damping is a key parameter, to which whirl flutter is extremely sensitive and which needs to be validated. Therefore, aeroelastic models are used. The important experiments were carried out in NASA Langley by Reed, Bennett, Kvaternik and many others [5 - 10]. Experimental research into whirl flutter is also reported in [11]. A comprehensive description of whirl flutter experimental research is provided in [12].
VZLU's previous experimental activities include aeroelastic wind tunnel testing in the frame of the Czech aircraft structures certification. Many experiments were carried out; however, these experiments did not include a rotating propeller. Aeroelastic models, that were formerly used for certification purposes, are currently often rebuilt, and utilized as research demonstrators for research of novel concepts, systems, methods, etc. An example of such a utilization is the model of the L-610 Czech turboprop commuter aircraft. The developed research demonstrator represents the half-wing and engine of a typical commuter turboprop aircraft structure. The model has three options: 1) The standard linear model with engine attachment with four degrees-of-freedom, 2) The nonlinear model with nonlinear attachment of the engine in pitch and nonlinear aileron actuation [13, 14] and 3) The whirl flutter model (W-WING) with a rotating propeller for investigation of the whirl flutter phenomenon [15 - 17].
The new option of the last demonstrator, that is described in this paper is a sting-mounted nacelle with a motor and propeller (W-STING). The demonstrator is utilized for investigation of a propeller aerodynamic derivatives. This paper includes the description of the mechanical concept of the demonstrator and the methodology of experimental

DOI: 10.13009/EUCASS2023-330

investigation of propeller aerodynamic derivatives.

2. Theoretical Background

The principle of the whirl flutter phenomenon is outlined on a simple mechanical system with two degrees-of-freedom [12]. The propeller and hub are considered to be rigid. A flexible engine mounting is substituted as a system of two rotational springs (stiffness K_Ψ, K_Θ), as illustrated in figure 1. Such a system has two independent mode shapes of yaw and pitch, with respective angular frequencies of ω_Ψ and ω_Θ. Considering the propeller rotation with angular velocity Ω, the primary system motion changes to the characteristic gyroscopic motion. The gyroscopic effect causes two independent mode shapes to merge into whirl motion. The propeller axis develops an elliptical movement. The trajectory of this elliptical movement depends on both angular frequencies ω_Ψ and ω_Θ. The orientation of the propeller axis movement is backward relative to the propeller rotation for the lower-frequency mode (backward whirl mode) and is forward relative to the propeller rotation for the higher-frequency mode (forward whirl mode). Because the yaw and pitch motions have a 90° phase shift, the mode shapes in the presence of gyroscopic effects are complex.

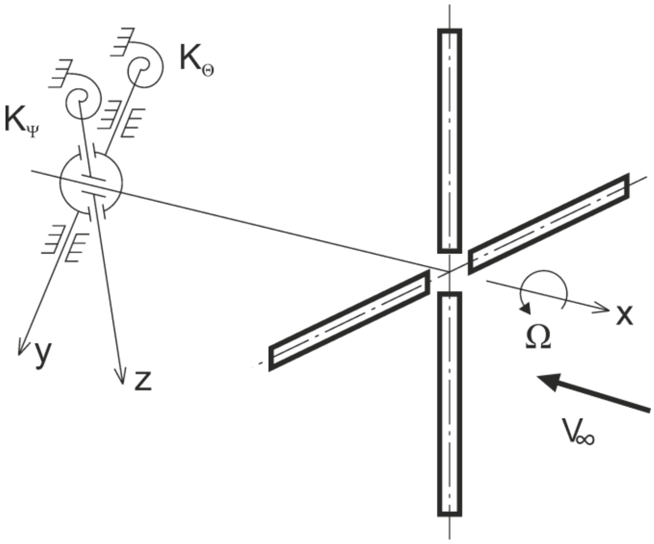

Figure 1: Gyroscopic system with a propeller.

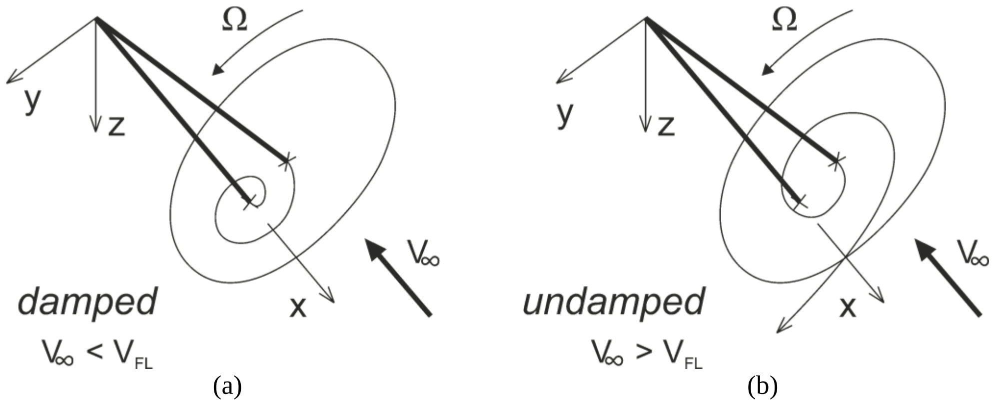

Figure 2. Stable (a) and unstable (b) state of gyroscopic vibrations for the backward flutter mode.

The described gyroscopic motion causes the angles of attack of the propeller blades to change, which consequently leads to unsteady aerodynamic forces. These forces may, under specific conditions, induce whirl flutter instability. The flutter state is defined as the neutral stability with no damping of the system, and the corresponding airflow ($V_\infty = V_{FL}$) is called the critical flutter speed. The possible states of the gyroscopic system from a flutter point of view for the backward mode are explained in figure 2. Provided that the air velocity is lower than a critical value ($V_\infty < V_{FL}$), the system is stable, and the gyroscopic motion is damped. If the airspeed exceeds the critical value ($V_\infty > V_{FL}$), then the system becomes unstable and gyroscopic motion is divergent.
The analytical solution is intended to determine the aerodynamic force caused by the gyroscopic motion on each of the propeller blades. The presented equations of motion were derived for the system shown in figure 1 using Lagrange's

DOI: 10.13009/EUCASS2023-330

approach. The kinematical scheme including gyroscopic effects is shown in figure 3. We select three angles (***φ***, ***Θ***, ***Ψ***) as the independent generalized coordinates. The propeller angular velocity is considered to be constant ($\varphi = \Omega t$). The rotating component is assumed to be cyclically symmetric with respect to both mass and aerodynamics (i.e., a propeller with a minimum of three blades). Non-uniform mass moments of inertia of the engine with respect to pitch and yaw axes ($J_Z \neq J_Y$) are also considered.

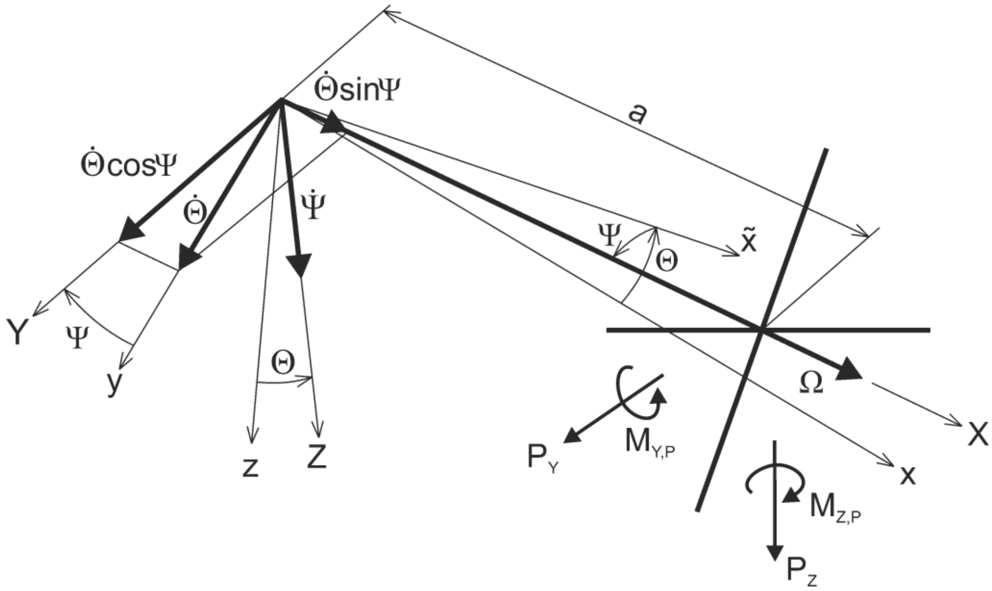

Figure 3: Kinematical scheme of the gyroscopic system

Considering small angles, the equations of motion become:

$$\begin{aligned} J_Y\ddot{\Theta} + (K_\Theta\gamma_\Theta/\omega)\dot{\Theta} + J_X\Omega\dot{\Psi} + K_\Theta\Theta &= M_{YP} - aP_Z \\ J_Z\ddot{\Psi} + (K_\Psi\gamma_\Psi/\omega)\dot{\Psi} + J_X\Omega\dot{\Theta} + K_\Psi\Psi &= M_{ZP} + aP_Y \end{aligned} \tag{1}$$

Propeller aerodynamic forces (right-hand side of eqn. 1, see also figure 3) are determined using aerodynamic derivatives [3, 18]. Neglecting the aerodynamic inertia terms, the equations for the propeller's dimensionless forces and moments may be expressed as follows:

$$\begin{aligned} P_Y = qS\left(c_{y\Psi}\Psi^* + c_{y\Theta}\Theta^* + c_{y\mathrm{q}}\left(\dot{\Theta}^* D/2V\right)\right) \quad & P_Z = qS\left(c_{z\Psi}\Psi^* + c_{z\Theta}\Theta^* + c_{zr}\left(\dot{\Psi}^* D/2V\right)\right) \\ M_{YP} = qSD\left(c_{m\Psi}\Psi^* + c_{m\mathrm{q}}\left(\dot{\Theta}^* D/2V\right)\right) \quad & M_{ZP} = qSD\left(c_{n\Theta}\Theta^* + c_{nr}\left(\dot{\Psi}^* D/2V\right)\right) \end{aligned} \tag{2}$$

Where ***q*** is a dynamic pressure, ***S*** is a propeller disc area, ***D*** is a propeller diameter and ***V*** is an airflow velocity. The aerodynamic derivatives (c-terms) are defined as follows:

$$\begin{aligned} c_{y\Theta} = \partial c_y/\partial\Theta^* \quad c_{y\Psi} = \partial c_y/\partial\Psi^* \quad c_{y\mathrm{q}} = \partial c_y/\partial\left(\dot{\Theta}D/2V\right) \quad c_{y\mathrm{r}} = \partial c_y/\partial\left(\dot{\Psi}D/2V\right) \\ c_{z\Theta} = \partial c_z/\partial\Theta^* \quad c_{z\Psi} = \partial c_z/\partial\Psi^* \quad c_{z\mathrm{q}} = \partial c_z/\partial\left(\dot{\Theta}D/2V\right) \quad c_{z\mathrm{r}} = \partial c_z/\partial\left(\dot{\Psi}D/2V\right) \\ c_{m\Theta} = \partial c_m/\partial\Theta^* \quad c_{m\Psi} = \partial c_m/\partial\Psi^* \quad c_{m\mathrm{q}} = \partial c_m/\partial\left(\dot{\Theta}D/2V\right) \quad c_{m\mathrm{r}} = \partial c_m/\partial\left(\dot{\Psi}D/2V\right) \\ c_{n\Theta} = \partial c_n/\partial\Theta^* \quad c_{n\Psi} = \partial c_n/\partial\Psi^* \quad c_{n\mathrm{q}} = \partial c_n/\partial\left(\dot{\Theta}D/2V\right) \quad c_{n\mathrm{r}} = \partial c_n/\partial\left(\dot{\Psi}D/2V\right) \end{aligned} \tag{3}$$

Considering the symmetry (or antisymmetry), we can reduce the number of derivatives as follows:

$$c_{z\Psi} = c_{y\Theta}\,;\, c_{m\Psi} = -c_{n\Theta}\,;\, c_{mq} = c_{nr}\,;\, c_{zr} = c_{yq}\,;\, c_{z\Theta} = -c_{y\Psi}\,;\, c_{n\Psi} = c_{m\Theta}\,;\, c_{mr} = -c_{nq}\,;\, c_{yr} = -c_{zq} \tag{4}$$

In addition, we can neglect the negligible derivatives: $c_{mr} = -c_{nq} = 0$ and $c_{yr} = -c_{zq} = 0$. Finally, we obtain six independent derivatives: $c_{z\Theta}$, $c_{m\Theta}$, $c_{z\Psi}$, $c_{m\Psi}$, c_{mq} and c_{zr}. The first four ones may be investigated experimentally.

DOI: 10.13009/EUCASS2023-330

Final solving for the critical (flutter) state assuming harmonic motion has the character of an eigenvalue problem. The final whirl flutter matrix equation can be expressed as:

$$\left(-\omega^2[M]+j\omega\left([D]+[G]+q_\infty F_P\frac{D_P^2}{V_\infty}\left[D^A\right]\right)+\left([K]+q_\infty F_P D_P\left[K^A\right]\right)\right)\begin{bmatrix}\overline{\Theta}\\ \overline{\Psi}\end{bmatrix}=\{0\} \tag{5}$$

The critical state emerges when the angular velocity **ω** is real. The critical state can be reached by increasing either V_∞ or Ω. Increasing the propeller advance ratio $(V_\infty/(\Omega R))$ has a destabilizing effect. Another important parameter is the distance between the propeller and the node points of the engine vibration modes. Structural damping is a significant stabilization factor, while in contrast, the influence of the propeller thrust is negligible. The small influence of the propeller thrust derives from the fact that the variance of the aerodynamic derivatives of the thrusted propeller and windmilling propeller can be high in the low-speed region, but at high velocities (where whirl flutter is expected), the variance is less than 5% [6]. The most critical state is $\omega_\Theta = \omega_\Psi$, when the interaction of both independent motions is maximal, and the trajectory of the gyroscopic motion is circular. Considering rigid propeller blades, the whirl flutter inherently appears in the backward gyroscopic mode. A special case of eqn. 5 for $\omega = 0$ is gyroscopic static divergence, which is characterized by uni-directional divergent motion. The described mathematical model that considers a rigid propeller is obviously applicable to conventional propellers, for which the propeller blade frequencies are much higher compared to the nacelle pitch and yaw frequencies.

3. Aeroelastic Demonstrator (W-STING)

Aeroelastic demonstrator for investigation of a propeller aerodynamic derivatives (W-STING) represents a sting-mounted nacelle with a motor and propeller. The demonstrator includes two degrees-of-freedom (engine pitch and yaw). For the measurement, just a single degree-of-freedom is used and other one is mechanically blocked. The stiffness parameters in both pitch and yaw are modelled by means of cross spring pivots with changeable spring leaves. Stiffness constants are independently adjustable by replacing these spring leaves. The leaf spring thickness ranges from 2.0 to 3.5 mm. The corresponding effective stiffness of the pitch hinge ranges from 246.4 to 1320.5 Nm.rad^{-1} and the engine pitch frequency ranges from 1.96 to 4.54 Hz. Both pivots can be independently moved in the direction of the propeller axis within the range of 0.15 m to adjust the pivot points of both vibration modes. The demonstrator is capable of simulating changes of all the important parameters influencing the whirl flutter. The inertia of the engine is modeled by the replaceable and movable (sliding) weight. It enables either to change the position of the center of gravity, or to preserve the center of gravity position in case the pivot stations change. The range of balance weight stations is 0.208 m. The plastic nacelle cowling is manufactured using the 3D print technology.

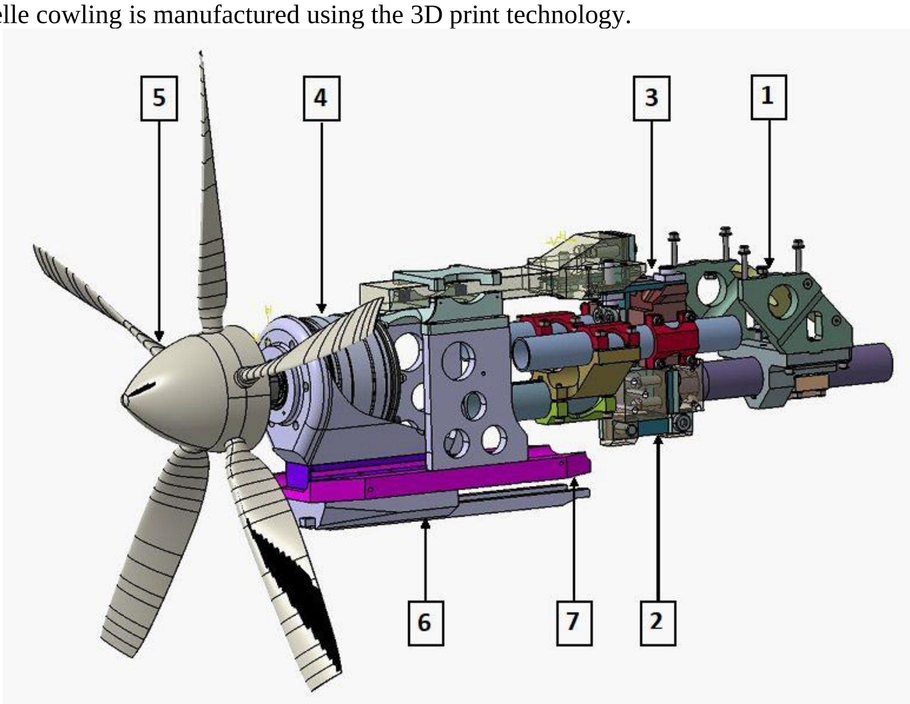

Figure 4: W-STING demonstrator, uncoated nacelle with motor and propeller (1 – sting attachment; 2 – yaw attachment; 3 – pitch attachment; 4 – motor; 5 – propeller; 6 – massbalance weight; 7 – thrust measurement cell).

DOI: 10.13009/EUCASS2023-330

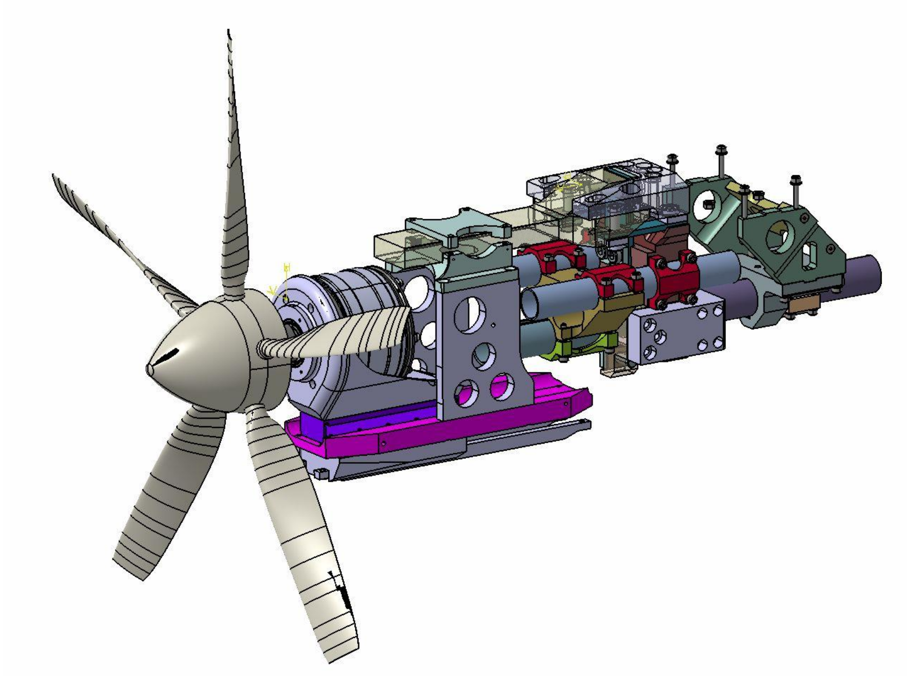

Figure 5: W-STING demonstrator, uncoated nacelle with motor and propeller, blocked yaw, and pitch degree-of-freedom.

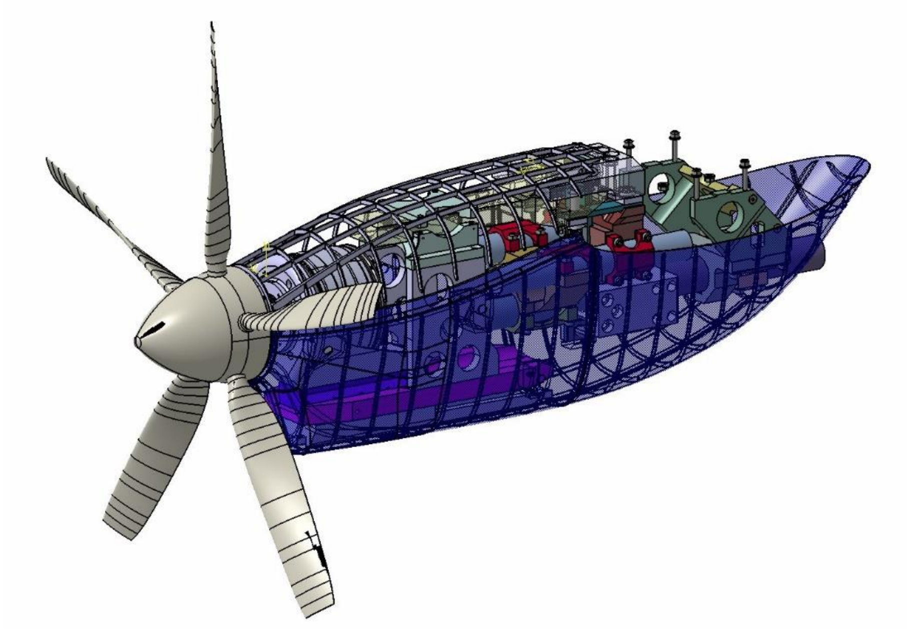

Figure 6: W-STING demonstrator, coated nacelle with motor and propeller.

The gyroscopic effect of the rotating mass is simulated by the mass of the propeller blades. Two sets of blades made of duralumin and steel are available. The polar moment of inertia of propeller with duralumin and steel blades is 0.0266 kg.m^2 and 0.0659 kg.m^2, respectively. The propeller with $\boldsymbol{D} = \mathbf{0.7\ m}$ represents a scaled-down real Avia V-518 5-blade propeller. The propeller blades' angle of attack is adjustable at the standstill by means of the special tool. The propeller is powered by an electric motor. The demonstrator sensor instrumentation includes measurements of both pitch and yaw angles using strain-gauge sensors and the measurement of both pitch and yaw pivot moments using the balance cell. In addition, propeller parameters (thrust, rpm, etc.) are measured as well. The system is controlled by the special in-house LabVIEW-based SW tool. The demonstrator design drawing is shown in figure 4. Figure 5 shows the state with blocked yaw and pitch degrees-of-freedom. Finally, figure 6 demonstrates the state of coated nacelle.

DOI: 10.13009/EUCASS2023-330

4. Methodology of Measurement

The static equations for the engine and propeller pitch and yaw deflection may be (from eqn. 1) expressed using the total moment-related derivatives (denoted by *) as:

$$k^2\Theta = \kappa(c^*_{m\Theta}\Theta + c^*_{m\Psi}\Psi) \qquad k^2\Psi = \kappa(c^*_{n\Psi}\Psi + c^*_{n\Theta}\Theta) \tag{5}$$

Note that the relations $\boldsymbol{c^*_{m\Theta} = c^*_{n\Psi}}$ and $\boldsymbol{c^*_{m\Psi} = -c^*_{n\Theta}}$ given by eqn. 4 were used in the latter equation. For determination of $\boldsymbol{c_{m\Theta}}$ (pitch moment due to pitch angle) and $\boldsymbol{c_{z\Theta}}$ (vertical force due to pitch angle) derivatives, the pitch-only arrangement of the demonstrator is used. Hence, for $\boldsymbol{\Psi = 0}$, the total pitching moment coefficient ($\boldsymbol{c^*_m}$) may be expressed as:

$$c^*_m = (K_\Theta\Theta/qSD) \tag{6}$$

Where $\boldsymbol{K_\Theta\Theta}$ is the measured pitch pivot moment. The measurement is performed varying the pitch angle (by manipulator) and the moment is evaluated with respect to the pitch angle ($\boldsymbol{\Theta}$). The slope of the measured curves is the reference total pitch moment due to pitch angle derivative ($\boldsymbol{c^*_{m\Theta}}$). To separate the force and moment contributions to the total pitch moment, two configurations varying the distance between the gimbal axis and the propeller plane ($\boldsymbol{a}$) are measured. The equations are:

$$c^*_{m\Theta1} = c_{m\Theta} - (a_1/D)c_{z\Theta} \qquad c^*_{m\Theta2} = c_{m\Theta} - (a_2/D)c_{z\Theta} \tag{7}$$

And the final expressions for the aerodynamic derivatives become:

$$c_{m\Theta} = \big(1/(a_2 - a_1)\big)(a_2c^*_{m\Theta1} - a_1c^*_{m\Theta2}) \qquad c_{z\Theta} = \big(D/(a_2 - a_1)\big)(c^*_{m\Theta1} - c^*_{m\Theta2}) \tag{8}$$

For determination of $\boldsymbol{c_{m\Psi}}$ (pitch moment due to yaw angle) and $\boldsymbol{c_{z\Psi}}$ (vertical force due to yaw angle) derivatives, the yaw-only arrangement of the demonstrator is used. Hence, the total yawing moment coefficient ($\boldsymbol{c^{**}_n}$) may be expressed as:

$$c^{**}_n = (K_\Psi\Psi/qSD) = (c^*_{n\Psi}\Psi + c^*_{n\Theta}\Theta) \tag{9}$$

Where $\boldsymbol{K_\Psi\Psi}$ is the measured yaw pivot moment. The measurement is performed varying the pitch angle (by manipulator) and the moment is evaluated with respect to this pitch angle ($\boldsymbol{\Theta}$). The slope of the measured curves ($\boldsymbol{c^{**}_{n\Theta}}$) and eqn. (9) are used to obtain the reference yaw total moment due to pitch angle derivative ($\boldsymbol{c^*_{n\Theta}}$) that is:

$$c^*_{n\Theta} = \big(c^{**}_{n\Theta} - c^*_{n\Psi}(\Psi/\Theta)\big) \tag{10}$$

The yaw-to-pitch angle ratio ($\boldsymbol{\Psi/\Theta}$) is constant just for a given blade angle and dynamic pressure. Since the ($\boldsymbol{\Psi/\Theta}$) ratio is dynamic pressure dependent, the yawing moment coefficient ($\boldsymbol{c^{**}_n}$) is dynamic pressure dependent as well. The reference total yaw moment due to yaw angle derivative ($\boldsymbol{c^*_{n\Psi}}$) is obtained using the antisymmetry (eqn. (4)) as $\boldsymbol{c^*_{n\Psi} = c^*_{m\Theta}}$. Similarly, we use $\boldsymbol{c^*_{n\Theta} = -c^*_{m\Psi}}$ to obtain the reference total pitch moment due to yaw angle derivative ($\boldsymbol{c^*_{m\Psi}}$). Separation of ($\boldsymbol{c^*_{m\Psi}}$) to its components ($\boldsymbol{c_{m\Psi}}$) and ($\boldsymbol{c_{z\Psi}}$), i.e., the separation of force and moment contributions is carried out similarly as mentioned above, i.e., by measuring of two configurations varying the distance between the gimbal axis and the propeller plane ($\boldsymbol{a}$). The final expressions for aerodynamic derivatives are:

$$c_{m\Psi} = \big(1/(a_2 - a_1)\big)(a_1c^*_{n\Theta2} - a_2c^*_{n\Theta1}) \qquad c_{z\Psi} = \big(D/(a_2 - a_1)\big)(c^*_{n\Theta2} - c^*_{n\Theta1}) \tag{11}$$

DOI: 10.13009/EUCASS2023-330

5. Conclusion and Outlook

The paper deals with the mechanical concept of the aeroelastic demonstrator for the measurement of a propeller aerodynamic derivatives (W-STING). The demonstrator represents a sting-mounted nacelle with the engine and thrusting propeller. The demonstrator's concept allows adjusting of all main parameters influencing whirl flutter. A broad testing campaign in the VZLU 3m-diameter wind tunnel is planned. The test schedule includes the measurement of four aerodynamic derivatives. Secondary variable parameters include the airflow velocity (dynamic pressure) and a blade angle of attack. The experimental results will be subsequently utilised for verification of the analytical models and computational tools [19, 20] that will be used for development of the new power plant system, characterised as an open-fan concept, utilised for a new generation short-medium range turboprop aircraft.

Acknowledgement

Program and topic: HORIZON-JU-CLEAN-AVIATION-2022-01-SMR-01, Ultra Efficient Propulsion Systems for Short and Short-Medium Range Aircraft. Project nr. and title: 101102011, Open Fan for Environmental Low Impact of Aviation (OFELIA).

References

[1] Taylor, E. S., and Browne, K. A. 1938. Vibration Isolation of Aircraft Power Plants, *J. Aerosp. Sci.*, 6(2):43-49.
[2] Ribner, H. S. 1945. Propellers in Yaw, NASA Rep. 820.
[3] Ribner, H. S. 1945. Formulas for Propellers in Yaw and Charts of the Side - Force Derivatives, NACA Rep. 819.
[4] Donham, R. E. and Watts, G. A. 1997. Whirl Flutter First Case, In: The Revolution in Structural Dynamics, (Editor Dr. Hugh Flomenhoft), Dynaflo Press, Palm Beach Gardens, FL, USA, 99-109.
[5] Reed, W. H., and Bland, S. R. 1961. An Analytical Treatment of Aircraft Propeller Precession Instability, NASA TN D-659.
[6] Reed, W. H. and Bennett, R. M. 1963. Propeller Whirl Flutter Considerations for V/STOL Aircraft, In: *CAL/TRECOM Symposium*, Buffalo, NY, USA.
[7] Bland, S. R. and Bennett, R. M. 1963. Wind-Tunnel Measurement of Propeller Whirl-Flutter Speeds and Static Stability Derivatives and Comparison with Theory, NASA TN D-1807.
[8] Bennett, R. M. and Bland, S. R. 1964. Experimental and Analytical Investigation of Propeller Whirl Flutter of a Power Plant on a Flexible Wing, NASA TN D-2399.
[9] Abbott, F.T., Jr., Kelly, H. N., Hampton, K. D. 1963. Investigation of Propeller-Power Plant Autoprecession Boundaries for a Dynamic-Aeroelastic Model of a Four-Engine Turboprop Transport Airplane, NASA, Technical Note, TN D-1806.
[10] Kvaternik, R. G., and Kohn, J. S. 1977. An Experimental and Analytical Investigation of Proprotor Whirl Flutter, NASA TP 1047.
[11] Krishna Rao, K. V. and Sundararajan, D. 1969. Whirl Flutter of Flapping Blade Rotor Systems, NAL TN-18, National Aeronautical Laboratory, Bangalore, India.
[12] Čečrdle, J. 2023. Whirl Flutter of Turboprop Aircraft Structures, 2nd Ed., Elsevier Science, Oxford, UK.
[13] Maleček, J., Hlavatý, V., Malínek, P. and Čečrdle, J. 2011. Development of Wing / Engine Component Non-linear Aeroelastic Demonstrator, In: *International Forum on Aeroelasticity and Structural Dynamics*, Paris, France.
[14] Maleček, J., Čečrdle, J., Hlavatý, V. and Malínek, P. 2013. Mechanical Concepts for Simulation of Nonlinearities on Aeroelastic Demonstrator, *J. Aircr.*, 50(2):651-658.
[15] Čečrdle, J. and Maleček, J. 2013. Mechanical Concept of W-WING Whirl Flutter Aeroelastic Demonstrator, *Proc. Institution of Mech. Engineers, Part G: J. Aerosp. Eng.*, 229(8):1485-1494.
[16] Čečrdle, J. – Malínek, P. and Vích, O. 2017. Wind Tunnel Test of a Whirl Flutter Aeroelastic Demonstrator, In: *Proc. AIAA SciTech Forum*, San Diego, CA, USA.
[17] Čečrdle, J. – Vích, O. and Malínek, P. 2019. Wind Tunnel Test of a Whirl Flutter Aeroelastic Demonstrator, *Proc. Institution of Mech. Engineers, Part G: J. Aerosp. Eng.*, 233(3):969-977.
[18] Houbolt, J. C. and Reed, W. H. 1962. Propeller Nacelle Whirl Flutter, *J. Aerosp. Sci.*, 29:333-346.
[19] Dugeai, A., Mauffrey, Y. and Sicot, F. 2011. Aeroelastic Capabilities of the elsA Solver for Rotating Machines Applications, In*: Int. Forum on Aeroelasticity and Structural Dynamics*, Paris, France.
[20] Sicot, F. and Dugeai, A. 2011. Numerical Investigation of Propellers Whirl Flutter Using elsA, In: *Int. Forum on Aeroelasticity and Structural Dynamics*, Paris, France.